

Resolution of Key Roles for the Distal Pocket Histidine in Cytochrome *c* Nitrite Reductases

Colin W. J. Lockwood^a, Benedicte Burlat^{a, †}, Myles R. Cheesman^a, Melanie Kern^c, Jörg Simon^c, Thomas A. Clarke^b, David J. Richardson^b and Julea N. Butt^{a,b*}

Centre for Molecular and Structural Biochemistry, ^a School of Chemistry and ^b School of Biological Sciences, University of East Anglia, Norwich Research Park, Norwich, NR4 7TJ, UK

^c Microbial Energy Conversion and Biotechnology, Department of Biology, Technische Universität Darmstadt, Schnittspahnstrasse 10, 64287 Darmstadt, Germany

ABSTRACT: Cytochrome *c* nitrite reductases perform a key step in the biogeochemical N-cycle by catalyzing the six-electron reduction of nitrite to ammonium. These multi-heme cytochromes contain a number of His/His ligated *c*-hemes for electron transfer and a structurally differentiated heme that provides the catalytic center. The catalytic heme has proximal ligation from lysine, or histidine, and an exchangeable distal ligand bound within a pocket that includes a conserved histidine. Here we describe properties of a penta-heme cytochrome *c* nitrite reductase in which the distal His has been substituted by Asn. The variant is unable to catalyze nitrite reduction despite retaining the ability to reduce a proposed intermediate in that process, namely, hydroxylamine. A combination of electrochemical, structural and spectroscopic studies reveals that the variant enzyme simultaneously binds nitrite and electrons at the catalytic heme. As a consequence the distal His is proposed to play a key role in orienting the nitrite for N-O bond cleavage. The electrochemical experiments also reveal that the distal His facilitates rapid nitrite binding to the catalytic heme of the native enzyme. Finally it is noted that the thermodynamic descriptions of nitrite- and electron-binding to the active site of the variant enzyme are modulated by the prevailing oxidation states of the His/His ligated hemes. This is behavior that is likely to be displayed by other multi-centered redox enzymes such that there are wide implications for considering the determinants of catalytic activity in this important and varied group of oxidoreductases.

INTRODUCTION

Nitrite reduction is a protein-catalyzed reaction performed for biological advantage in all kingdoms of life ¹. At the present time at least eleven nitrite-reducing hemoproteins are known and their utility is readily illustrated through a few examples. In humans these enzymes produce nitric oxide to mediate a spectrum of physiological responses in blood and tissue. In plants such proteins produce ammonium for the synthesis of N-containing biomolecules. In bacteria the nitrite-reducing hemoproteins produce either nitric oxide or ammonium in support of energy conservation, detoxification and N-assimilation. From this brief survey it is apparent that nitrite-reducing cytochromes selectively catalyze the one-electron, two-proton conversion to nitric oxide or the six-electron, eight-proton transformation that produces ammonium. As a consequence there is much interest in defining the molecular determinants of catalysis across this group of enzymes.

The bacterial cytochrome *c* nitrite reductases produce ammonium. In so doing these proteins perform a transformation that in other circumstances requires four different enzymes with nitric oxide, nitrous oxide and di-nitrogen as discrete intermediates ^{2,3}. Nevertheless, or perhaps because of this, the nitrite ammonification reaction as

catalyzed by cytochrome *c* nitrite reductases occurs with turnover frequencies exceeding 500 s⁻¹ and without the release of detectable intermediates ⁴⁻⁸. Several structurally conserved features serve to underpin this behavior ⁷⁻¹³. Rapid intraprotein electron transfer is secured by a constellation of five closely-packed *c*-type hemes with adjacent Fe-Fe distances < 13 Å as illustrated for the homo-dimeric *Escherichia coli* enzyme in Fig. 1. Four of these hemes have His/His ligation while the fifth heme is structurally differentiated to provide the catalytic center, e.g. Fig. 1 inset. The latter heme has proximal ligation from lysine or histidine ¹⁴. The distal ligand is exchangeable and bound within a pocket defined by the side chains of three conserved residues, namely, His, Tyr and Arg.

Possible catalytic contributions of the distal pocket residues have been considered by computational analyses ¹⁵⁻¹⁸. A key intermediate was taken to be Fe-N(NO₂). This species was resolved in X-ray diffraction of the cytochrome *c* nitrite reductase from *Wolinella succinogenes* where the nitrite is oriented by H-bonds to the distal His and Arg residues. Protonation and subsequent cleavage of an N-O bond in the first committed step of catalysis would be facilitated by maximizing the negative charge on the nitrite oxygens through iron-to-nitrite back-bonding. This bonding was found to be maximized with the nitrite oriented to form H-bonds with the

His (N_ϵ) and Arg ($N_{\epsilon 2}$) residues as resolved by X-ray diffraction. From this structure two possible routes for N-O bond cleavage were proposed. One pathway utilized the His side chain as the proton donor. In the second pathway, the role of proton donor was taken by the Arg side chain when the distal His was deprotonated.

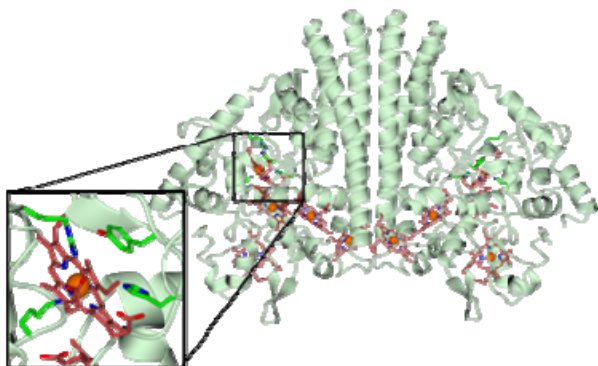


Figure 1. Crystal structure of the cytochrome *c* nitrite reductase, NrfA, from *E. coli*. Inset, active site highlighting the catalytic triad of Arg106, Tyr216 and His264 in addition to the Lys126 distal heme ligand. Image rendered in ccp4mg from PDB entry 2RDZ.

As the example above illustrates, density functional analysis provides invaluable insight into the possible roles of the distal pocket residues during catalysis and the distribution of charge across the heme cofactor and its axial ligands. However, in terms of defining catalytic rate such analyses are necessarily blind to the contributions made by the electrostatic potential of the protein and the diffusion of molecules and ions between active site and bulk solvent. The latter may be particularly relevant for cytochrome *c* nitrite reductases where solvent filled channels extend through the protein to link the distal face of the catalytic heme to the protein exterior. As a consequence we have prepared and characterized two cytochrome *c* nitrite reductases in which the conserved distal His has been replaced by Asn. Neither variant reduces nitrite at a detectable rate. However, both variants retain the ability to reduce hydroxylamine which is a proposed intermediate of nitrite reduction, see ¹⁵ and references therein. To understand the basis of this behavior a series of synergistic spectroscopic, structural and electrochemical investigations were performed. The studies shed fresh light on the mechanisms by which nitrite is transported to, and subsequently processed by, the active site of cytochrome *c* nitrite reductases in results that have wide-ranging implications for understanding the catalytic properties of multi-centered redox enzymes.

METHODS

Materials. Two cytochrome *c* nitrite reductase variants were prepared in which the distal His was replaced by Asn, namely, *Ec* His264Asn NrfA and *Ws* His277Asn NrfA. These proteins were derived from the native enzymes of the human pathogenic γ -proteobacterium *E. coli* and the non-pathogenic rumen ϵ -proteobacterium *W. succinogenes*, respectively. Changes encoding for the His264Asn substitution were introduced into *E. coli nrfA* using the Quikchange qSite-

Directed Mutagenesis kit (Stratagene) following the manufacturer's instructions and using the plasmid pJG1 as the template ¹⁹. The forward primer was GCCAATGCTGAAAGC GCAGACCCGGAATATGAAACCTG (codon 264 underlined, substitution in bold). To access *Ec* His264Asn NrfA, the plasmid encoding for this protein (pJG1.H264N) was transformed into *E. coli* strain JCB4083a cells that have the genotype $\Delta narZ::\omega \Delta narL::Tn10 \Delta napGH \Delta nrfAB \Delta nirBDC::Kan^R$ and contain the cytochrome *c* maturation plasmid pEC86 ²⁰. A previously published procedure was used to purify *Ec* His264Asn NrfA from the transformed cells ^{19,21}. Protein concentrations were defined using $\epsilon_{410nm} = 497\ 650\ M^{-1}\ cm^{-1}$ for the oxidized protein ⁸. The method used to introduce the His277Asn substitution in *W. succinogenes* NrfA was based on a published strategy ²² using plasmid pMK11-*Ws*NrfA_H277N and as described in the Supporting Information. *Ws* His277Asn NrfA was subsequently purified from the corresponding *W. succinogenes* mutant cells via one-step chromatography using a Strep-Tactin H-PR cartridge (IBA GmbH) following the manufacturer's protocol. Purified protein was quantified using the bicinchoninic acid protein assay kit (Novagen) with bovine serum albumin as standard.

All other reagents were of Analar quality or higher and the water used had resistivity $> 18\ M\Omega\ cm$. Stock solutions of $NaNO_2$ (1 M) and $H_2NOH.HCl$ (2 M) were prepared in the desired buffer-electrolyte as needed for each day of experiments.

Protein Structure Determination. Crystals of *Ec* His264Asn NrfA were grown and harvested using a previously described method ¹⁹. *Ec* His264Asn NrfA crystals were immersed in a cryoprotected solution containing 50 mM nitrite for 15 minutes before flash cooling in liquid nitrogen to obtain nitrite-soaked *Ec* His264Asn NrfA crystals. X-ray diffraction data was collected on cryoprotected crystals at an X-ray wavelength of 0.9778 Å using beamline I24 at the Diamond Light Source (Oxford, UK). *Ec* His264Asn NrfA crystals diffracted to a final resolution of 2.15 Å and were of space group $P2_12_12_1$ with dimensions $a = 42.24\ \text{Å}$, $b = 89.49\ \text{Å}$ and $c = 274.72\ \text{Å}$, and $\alpha = \beta = \gamma = 90^\circ$. Nitrite soaked crystals were of an isomorphous space group and diffracted to a final resolution of 2.2 Å with cell dimensions of $a = 42.04\ \text{Å}$, $b = 89.44\ \text{Å}$ and $c = 273.42\ \text{Å}$. Data were processed using Xia2 ²³ as part of the CCP4 package ²⁴ and data collection statistics for *Ec* His264Asn NrfA are summarized in SI Table 1. Phases were obtained by molecular replacement using a single monomer from the 1.7 Å resolution structure of *Ec* NrfA as the search model (PDB entry 2RDZ) ¹⁹ and as described in the Supporting Information. The refined coordinates were deposited to the Protein Data Bank with accession number 4WJY.

Measurements of Catalytic Activity. Spectrophotometric assays of cytochrome *c* nitrite reductase activity measured the rate of viologen oxidation due to nitrite or hydroxylamine reduction initiated by the addition of enzyme ²¹. Assays used dithionite reduced methyl viologen ($\epsilon_{600nm} = 13.7\ mM^{-1}\ cm^{-1}$) or benzyl viologen ($\epsilon_{546nm} = 9.75\ mM^{-1}\ cm^{-1}$) for the *Ec* and *Ws* enzymes respectively. Resolution of the catalytic activity of *Ec* His264Asn NrfA by protein-film electrochemistry used the approach described previously for the native enzyme ²⁵⁻²⁷. Rotation of the pyrolytic graphite edge (PGE) working electrode at 3000 rpm ensured that the catalytic currents (i_{cat})

describing hydroxylamine reduction were free from limitation by the rate of substrate delivery to the electrode surface. Values of i_{cat} measured at -0.5 V were corrected for a first order loss of magnitude with time using the previously described method^{25,26} and then values of K_M and i_{max} (equivalent to V_{max}) were obtained from Lineweaver-Burk plots through fits to the equation:

$$\frac{1}{i_{\text{cat}}} = \frac{1}{i_{\text{max}}} + \frac{K_M}{i_{\text{max}}} \frac{1}{[\text{hydroxylamine}]}$$

The dissociation constant (K_d^{red}) describing nitrite binding as a competitive inhibitor of hydroxylamine reduction at -0.5 V applied potential was quantified through the equation:

$$K_M^{\text{obs}} = K_M + \frac{K_M}{K_d^{\text{red}}} [\text{NO}_2^-]$$

where K_M^{obs} is the value of K_M measured in the presence of nitrite.

Spectroscopic Assessment of Nitrite Binding to Solutions of Protein. Nitrite binding to the *E. coli* enzymes was monitored by electronic absorbance and electron paramagnetic resonance (EPR) spectroscopies. Values for the dissociation constant, K_d^{ox} , describing nitrite binding to oxidized enzyme were determined from variation of the magnitudes of the appropriate spectral features with nitrite concentration using the equation

$$\frac{[\text{NrfA:NO}_2^-]}{[\text{NrfA}]_{\text{total}}} = \frac{(C - \sqrt{C^2 - 4[\text{NrfA}]_{\text{total}}[\text{NO}_2^-]_{\text{total}}})}{2}$$

where $[\text{NrfA:NO}_2^-]$ is the concentration at equilibrium of the complex formed between nitrite and protein, $[\text{NrfA}]_{\text{total}}$ and $[\text{NO}_2^-]_{\text{total}}$ are the total concentration of protein and nitrite, respectively, and $C = [\text{NrfA}]_{\text{total}} + [\text{NO}_2^-]_{\text{total}} + K_d^{\text{ox}}$.

Spectroelectrochemistry. Spectroelectrochemistry of proteins adsorbed on optically transparent, mesoporous, nanocrystalline SnO_2 electrodes was performed in a three-electrode cell with minor modification of the previously described procedure²⁸. The quality of the spectral data was enhanced by placing a bare SnO_2 electrode in the reference beam to minimize spectral contributions from scattering by the nanocrystalline electrode material. Two methods were employed to define the redox properties of the hemes. In a potentiometric approach the electronic absorbance spectrum of the adsorbed protein was measured after poisoning at a desired potential for a given time. Redox transformations of the low- and high-spin hemes were also observed during cyclic voltammetry at 5 mV s^{-1} by simultaneously monitoring the absorbance at 552 or 442 nm, respectively. Comparable descriptions of the heme redox chemistry were obtained from both methods and the data that conveys the salient information with most clarity is presented here. Data justifying the wavelengths chosen for analysis of the high- and low-spin hemes in *Ec* His264Asn NrfA is presented in the Supporting Information.

When the heme redox transformations equilibrated fully on the timescale of the experiment it was possible to define heme reduction potentials. For spectra collected from a potentiometric approach the extent of heme reduction at each

potential was calculated from the difference in absorbance at two wavelengths, namely, $A_{552\text{nm}} - A_{582\text{nm}}$ for the low-spin hemes and $A_{442\text{nm}} - A_{452\text{nm}}$ for the high-spin heme. Heme reduction potentials were then defined using the equation

$$\Psi = \sum_{i=1}^j \frac{1}{j(1 + \theta_i)}$$

with $j = 4$ for the low-spin hemes and $j = 1$ for the high-spin heme. Ψ is the fractional reduction, $\theta_i = \exp(F(E - E_m^i)/RT)$, E is the electrode potential, E_m^i is the reduction potential of center i and the symbols F , R and T have their usual meaning. This equation describes the behavior when j independent centers undergo single-electron ($n = 1$) redox processes in accord with the Nernst equation and that contribute equally to the total change in absorbance. For data collected during cyclic voltammetry at 5 mV s^{-1} by monitoring $A_{552\text{nm}}$ or $A_{442\text{nm}}$, E_m values were derived from the first derivative of each absorbance with respect to applied potential (dA/dE) fit to the equation

$$\frac{dA}{dE} = \sum_{i=1}^j \frac{F^2 a \theta_i}{RT(1 + \theta_i)^2}$$

where a is a scaling parameter. Fits to the peaks detected for the reductive and oxidative sweeps gave two sets of apparent reduction potentials. These values were averaged, in pairs from highest to lowest potential, to report the E_m values for the relevant hemes. To quantify proton binding associated with redox transformation of the active site heme in *Ec* NrfA the plot of E_m versus pH was fit to the equation

$$E_m = E_{\text{alk}} + \frac{2.303RT}{nF} \log \left(\left[1 + \frac{[\text{H}^+]}{K_a^{\text{red}}} \right] / \left[1 + \frac{[\text{H}^+]}{K_a^{\text{ox}}} \right] \right)$$

where E_{alk} is the pH independent reduction potential at alkaline pH, and K_a^{ox} and K_a^{red} describe proton binding to the ferric and ferrous states of the high-spin heme respectively. All potentials are quoted versus standard hydrogen electrode (SHE).

Redox transformation of the *Ec* His264Asn NrfA high-spin heme in solutions of 5 and 50 μM nitrite did not reach equilibrium on the time-scale of the experiments described here. To describe the redox properties of the hemes under these conditions cyclic voltammetry (5 mV s^{-1}) was initiated at positive potential and the sweep paused at a series of desired potentials during its progress. Three minutes into each pause the electronic absorbance of the protein was measured. Following this cyclic voltammetry was resumed until the potential reached the next pause potential. This protocol imposed defined potential on the protein at all times in the experiment to ensure progressive reduction and then re-oxidation of the hemes.

Table 1: Kinetic parameters describing catalysis by NrfA enzymes.

		Nitrite		Hydroxylamine	
		k_{cat} (s^{-1})	K_M^a (μM)	k_{cat} (s^{-1})	K_M^a (μM)
<i>W. succinogenes</i> NrfA ^c	Native	758 ± 17	80 ± 16	215 ± 11	2 012 ± 31
	His277Asn	nd ^b	nd ^b	197 ± 16	2 029 ± 28
<i>E. coli</i> NrfA ^d	Native	1 350 ± 50	46 ± 4 (37 ± 5)	3 160 ± 123	30 000 ± 7 000 (128 000 ± 6 000)
	His264Asn	nd ^b	nd ^b	3 100 ± 900	170 000 ± 60 000 (130 000 ± 6 000)

^a Values in parenthesis defined by protein film electrochemistry at -0.5 V all other values from a spectrophotometric assay employing dithionite reduced viologen as electron donor. ^b No detected activity. ^c Measured in 50 mM potassium phosphate, pH 7. ^d Measured in 2 mM CaCl₂, 50 mM HEPES, pH 7.

RESULTS

Catalytic Consequences of Substituting His with Asn in the Distal Pocket of the Cytochrome *c* Nitrite Reductases from *Escherichia coli* and *Wolinella succinogenes*.

The pentaheme cytochrome *c* nitrite reductases (NrfA) from *E. coli* and *W. succinogenes* have proximal lysine ligation of the catalytic heme and have been extensively studied by a variety of methods, see for example ^{8,9,25-29} and references therein. As a consequence and in order to probe the contribution(s) of the distal His to catalysis we prepared a variant of each of these enzymes in which the corresponding His was replaced by Asn, namely, *Ec* His264Asn NrfA and *Ws* His277Asn NrfA. In spectrophotometric assays using dithionite reduced viologen as the electron donor it was immediately apparent that neither variant displayed detectable nitrite reductase activity, Table 1. However, the reduction of a proposed intermediate¹⁵ in nitrite reduction, namely, hydroxylamine, proceeded rapidly, Table 1. Our finding that the distal His plays a key role in nitrite reduction is supported by the very recent report of a 100-fold drop in nitrite reductase activity when the corresponding His is replaced by Gln in the cytochrome *c* nitrite reductase from *Shewanella oneidensis*³⁰.

Given the similar behaviors reported for substitution of the distal His in these homologous enzymes our subsequent studies to define their mechanistic basis were focused on the enzyme from *E. coli*. The flow of catalytic current (i_{cat}) in protein-film electrochemistry of *Ec* NrfA has been employed previously to resolve the dependence of this enzyme's catalytic rate on variables such as electrochemical potential, time, pH, substrate identity and substrate concentration ^{25,26,31}. Simply by comparing the shape, potential window and magnitude of the catalytic waveform in different conditions much valuable insight into the properties of the enzyme was available and this was despite the absence of detectable non-turnover waves that would allow k_{cat} to be quantified. The hydroxylamine reductase activity of *Ec* His264Asn NrfA was found to be similarly amenable to interrogation by protein-film electrochemistry, e.g. Fig. 2A. There was no discernable evidence for nitrite reduction (not shown).

A striking and consistent feature of the cyclic voltammograms describing hydroxylamine reduction by *Ec* His264Asn NrfA

was hysteresis in the catalytic current magnitudes of the forward and reverse potential sweeps, e.g. Fig. 2A. Smaller catalytic currents were displayed between approximately -0.25 and -0.4 V on sweeping to more negative potentials than were measured on returning to more positive potentials. This behavior is not displayed by *Ec* NrfA²⁵.

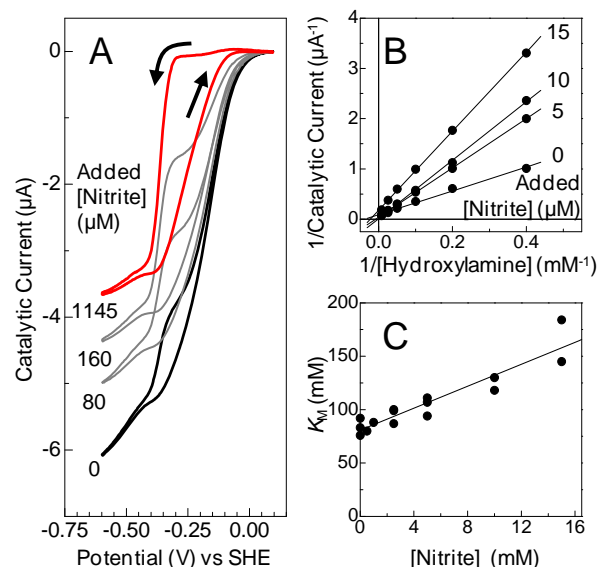


Figure 2. Nitrite inhibition of hydroxylamine reduction catalyzed by *Ec* His264Asn NrfA. (A) The catalytic current recorded during cyclic voltammetry of His264Asn NrfA adsorbed on PGE electrodes in the presence of 30 mM hydroxylamine and 0, 80, 160 or 1145 μM nitrite as indicated. The second voltammogram recorded at each nitrite concentration is shown and the arrows indicate scan direction for the voltammogram in 1145 μM nitrite. Scan rate 30 mV s^{-1} with electrode rotation at 3000 rpm. (B) Lineweaver-Burk plots for the catalytic currents at -0.5 V describing hydroxylamine reduction in solutions of 0, 5, 10 and 15 mM nitrite as indicated. Lines are linear fits to the Michaelis-Menten equation. (C) Variation of K_M with nitrite concentration where the line shows the behavior expected if nitrite acts as a competitive inhibitor of hydroxylamine reduction and described by $K_d = 15\,700\ \mu\text{M}$. Experiments performed in 2 mM CaCl₂, 50 mM HEPES, pH 7, 20°C

As will become apparent below, elaboration of the electrochemical experiment to define the origin of this hysteresis together with complementary structural and spectroscopic analyses provided unique insights into the multiple contributions that the distal pocket His makes to nitrite reduction. At this stage we limit ourselves to commenting on the information contained in the catalytic currents (i_{cat}) measured at potentials ≤ -0.5 V. These currents are essentially independent of scan direction so that they can be taken as a measure of steady-state catalysis by the adsorbed enzyme. The variation of $i_{\text{cat}}(-0.5$ V) with hydroxylamine concentration is well-described by the Michaelis-Menten equation, Fig. 2B, to yield a K_M value of the order of 130 000 μM . This is a value in good agreement with that obtained using the spectrophotometric assay and protein-film electrochemistry of *Ec* NrfA, Table 1. A slightly lower K_M describing hydroxylamine reduction by *Ec* NrfA in spectrophotometric assays was reported previously^{8,25} and also observed as part of this study. This may reflect differences between the solution and adsorbed states of the protein, i.e. local pH, dielectric and/or dynamic constraints, to which *Ec* His264Asn NrfA is less sensitive. Never the less it is clear that the kinetic constants describing hydroxylamine reduction by the native and variant enzymes are broadly similar regardless of the method used to define them. As a consequence we consider that the behavior of the adsorbed enzymes can be extrapolated to describe the key properties of these enzymes in solution.

Structural characterization of *Ec* His264Asn NrfA. To provide structural context for the properties of *Ec* His264Asn NrfA its crystal structure was resolved to 2.15 Å. This revealed a homodimeric protein and constellation of His/His and Lys-coordinated *c*-hemes indistinguishable from those of the native enzyme. Alignment of the α -carbon atoms in the variant and native proteins generated overlapping structures with an average rmsd of 0.31 ± 0.01 Å that confirmed their structural similarity. The successful introduction of Asn at position 264 within the active site was confirmed by an unbiased electron density map in which the electron density of that residue was well-described by Asn but not His, Fig. 3. Unambiguous assignment of the Asn side chain orientation was prevented by the similar electron densities of O and N. However, orienting the carbamide N nearer to the propionate at position 6 of the active site heme as illustrated in Fig. 3A would allow for weak H-bonds (3.6 Å) to form between these groups such that this is likely to represent the favored orientation. Asn264 and His264 adopt similar positions within the enzyme active sites and both residues are outliers in the Ramachandran plots describing the dihedral angles for their respective proteins, Supporting Information Fig. 1. This finding supports the hypothesis that the orientation of this residue is defined by steric constraints within the distal pocket rather than intrinsic properties of the side chain¹².

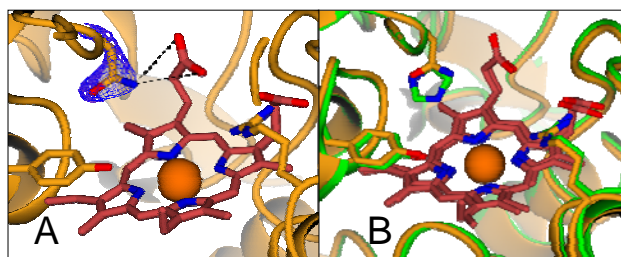


Figure 3. The active sites of His264Asn and native NrfA from *E. coli*. (A) Active site of His264Asn NrfA at 2.15 Å resolution. An unbiased simulated annealing F_0-F_c composite omit map contoured at 1.2σ (blue mesh) is shown for residue 264. Hydrogen-bonds from Arg264 to heme propionate are indicated with broken lines. (B) Superposition of the His264Asn (yellow) and native (green) NrfA active sites. Images rendered in ccp4mg from PDB entries 4WJY (His264Asn NrfA) and 2RDZ (native NrfA).

Previous crystallographic analysis of *Ec* NrfA suggested that the active site heme in the as isolated protein receives distal ligation from water or hydroxide⁸. This was corroborated by the electronic absorbance of a concentrated solution of the oxidized protein that contained a positive feature with a maximum at 630 nm⁸. High-spin ferric hemes display ligand-to-metal charge-transfer (LMCT) bands between 600 and 700 nm where there are no contributions from their low-spin counterparts³². The energy of these bands is diagnostic of the chemical nature of the axial ligands. For *Ec* NrfA the 630 nm band is indicative of hexa-coordinate heme with ligation from water (hydroxide) and lysine. By contrast *Ec* His264Asn NrfA displays a LMCT band centered on approximately 655 nm and indicative of penta-coordinate heme with a single nitrogenous axial ligand, Fig. 4A (continuous black line). In addition, the electron density within the active site of the crystallized protein indicates only partial occupancy of the distal ligation site. It was concluded that while *Ec* His264Asn NrfA retains the defining structural features of *Ec* NrfA these two proteins differ in their distal ligation of the catalytic heme.

***Ec* His264Asn NrfA Binds Nitrite.** The structural characterization of *Ec* His264Asn NrfA suggests the lack of nitrite reductase activity may arise because nitrite either fails to bind the protein, or, binds in an orientation/location incompatible with reductive N-O bond cleavage. To gain insight into these possibilities a solution of oxidized *Ec* His264Asn NrfA was equilibrated with increasing concentrations of nitrite and monitored by electronic absorbance spectroscopy, Fig. 4A. As the nitrite concentration was raised to 0.529 mM the LMCT band centered on 655 nm decreased in intensity. A new band appeared centered on 640 nm and a single set of isosbestic points were present in the overlaid spectra. Saturation of the nitrite binding site was confirmed when the spectrum was unchanged by further additions of nitrite.

Displacement of the LMCT-band maximum from 655 to 640 nm on nitrite binding is consistent with conversion of the penta-coordinate high-spin heme to a hexa-coordinate state. Because a maximum at 630 nm is displayed by the corresponding water (hydroxide) ligated heme in *Ec* NrfA it is most likely that nitrite binds as the distal heme ligand in *Ec* His264Asn NrfA. The affinity of nitrite for the NrfA variant is

quantified through the variation of absorbance at 640 nm with nitrite concentration. This relationship is well-described by the behavior expected for reversible 1 to 1 binding with a dissociation constant, K_d^{ox} , of $48 \pm 15 \mu\text{M}$, Fig. 4C. For comparative purposes solutions of oxidized *Ec* NrfA were also equilibrated with up to 3.5 mM nitrite but only very minor changes in the electronic absorbance of the protein were detected. As a consequence EPR spectroscopy was employed as a more sensitive probe of active site ligation, Fig. 4B. X-band EPR of *Ec* NrfA is dominated by a resonance at $g \approx 3.6$ that arises from a spin-coupled pair comprised of the high-spin ferric heme and a neighboring low-spin ferric heme^{26,33}. The magnitude of this resonance is very sensitive to the nature of the distal ligand to the high-spin ferric heme. Equilibrating *Ec* NrfA with increasing concentrations of nitrite decreased the magnitude of the $g \approx 3.6$ resonance in a manner well-described by the behavior expected for reversible 1 to 1 binding of nitrite with $K_d^{ox} = 395 \pm 50 \mu\text{M}$, Fig. 4C.

Having established that nitrite binds to oxidized *Ec* His264Asn NrfA with a moderately higher affinity than to *Ec* NrfA under the conditions of neutral pH used in these studies we turned our attention to assessing whether nitrite can bind to reduced, catalytically competent forms of the variant enzyme. Protein-film electrochemistry was employed for this purpose, e.g., Fig. 2A. The catalytic currents due to hydroxylamine reduction were significantly diminished by the introduction of nitrite. Analysis of $i_{cat}(-0.5 \text{ V})$ as a function of nitrite and hydroxylamine concentrations revealed nitrite to be a competitive inhibitor of hydroxylamine reduction, Fig. 2B. The linear variation of the observed K_M with nitrite concentration resolved a dissociation constant, K_d^{red} , of $15\,700 \pm 1\,200 \mu\text{M}$ for nitrite binding to reduced, catalytically competent *Ec* His264Asn NrfA, Fig. 2C.

Our results demonstrate nitrite binding to the catalytic heme in oxidized and reduced forms of *Ec* His264Asn NrfA. The implications of this behavior for the mechanism of nitrite reduction by the native enzyme are considered in the Discussion below. Here we consider two predictions arising from our observations. First, the much higher affinity of nitrite for oxidized over reduced forms of *Ec* His264Asn NrfA should result in a more negative reduction potential for the catalytic heme when nitrite is bound to this enzyme. Second, the hysteresis observed in the catalytic current-potential profiles describing hydroxylamine reduction by *Ec* His264Asn NrfA could be explained by ordered (un-)binding of electrons and nitrite at the active site and on the time-scale of the cyclic voltammetry. Specifically, dissociation of nitrite on the sweep to more negative potentials would alleviate inhibition and re-binding of nitrite on the sweep to more positive potentials would re-impose inhibition. This would explain the significantly increased hysteresis noted in voltammetry recorded at the higher nitrite concentrations, Fig. 2A. The hysteresis that is detected prior to nitrite addition can be attributed to the trace nitrite in the water and/or hydroxylamine stock solutions³⁴. This proposal would also explain the behavior noted over consecutive cyclic voltammograms and for different scan rates, Supporting Information Fig 2. As described below these predictions were confirmed through elaboration of the protein-film electrochemistry in a series of experiments revealing that the

distal His plays a key role in facilitating rapid, high-affinity binding of nitrite, and protons, to the active site of the native enzyme.

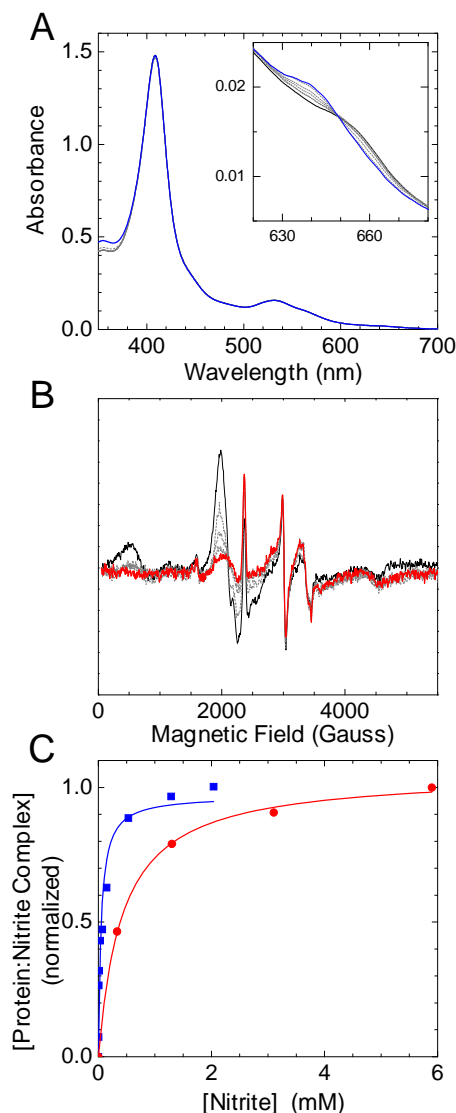


Figure 4. Spectroscopic analysis of nitrite-equilibrated His264Asn and native *E. coli* NrfA enzymes. (A) Electronic absorbance of oxidized 3 μM His264Asn NrfA equilibrated with 0 (continuous black line), 0.008, 0.016, 0.70, 0.147, 0.529 (broken lines) and 2.039 mM nitrite (blue line) in 2 mM CaCl_2 , 50 mM HEPES, pH 7. (B) EPR spectra of oxidized 70 μM native NrfA equilibrated with 0 (continuous black line), 0.33, 1.3, 3.1 (broken lines) and 5.9 mM nitrite (red line) in 50 mM HEPES, deuterated water, pH 7. Spectral measurements at 10 K with microwave frequency 9.66 GHz, modulation amplitude 10 Gauss and 2 mW power. (C) Fraction of His264Asn NrfA:nitrite (blue squares) and NrfA:nitrite (red circles) complexes as a function of nitrite concentration and normalized to the total enzyme concentration. The lines shown the behavior predicted for reversible, 1 to 1 complex formation with a K_d of 48 μM for His264Asn NrfA and 395 μM for NrfA.

Redox Driven (Un)-binding of Nitrite and Protons to *Ec* His264Asn NrfA.

We have previously characterized the redox properties of *Ec* NrfA through (magneto-)optical studies of protein solutions and protein adsorbed on optically transparent SnO₂ electrodes²⁸. The results were in good agreement but the latter method required less protein and the experiments were completed in a shorter time. As a consequence the redox properties of *Ec* His264Asn NrfA were resolved with the protein adsorbed as an electroactive film on optically-transparent SnO₂ electrodes. Variation of the electrode potential drove ferric/ferrous transformations of the high- and low-spin hemes that were monitored by the change in electronic absorbance (*A*) at 442 and 552 nm respectively as described in the Supporting Information. The transformations were fully reversible for a wide range of pH as summarized in plots of the first derivative of the absorbance with respect to applied potential (*dA/dE*) measured during cyclic voltammetry at 5 mV s⁻¹, e.g. Fig. 5A. Redox transformation of the high-spin heme in *Ec* His264Asn NrfA shows little variation with pH, Fig. 5B. By contrast *E_m* values for the corresponding heme in *Ec* NrfA show a pH dependence that is indicative of an *n* = 1 redox center binding a proton more tightly to its reduced, *pK_a^{red}* = 8.1, than its oxidized, *pK_a^{ox}* = 5.8, state, Fig. 5B. It can be concluded that the distal His allows for redox driven (de-)protonation of the active site in cytochrome *c* nitrite reductase as suggested by studies of a complex containing *Desulfovibrio desulfuricans* NrfA³⁵.

At neutral pH, reduction of the *Ec* His264Asn NrfA active site occurs without an accompanying protonation to offset the accumulated negative charge. As a consequence the significant drop in nitrite binding affinity that accompanies reduction of this enzyme can be explained simply on the basis of electrostatics. Experiments performed at pH 7 but with several different nitrite concentrations revealed the impact of nitrite on the redox properties of *Ec* His264Asn NrfA, e.g. Fig. 5A and 6. Following equilibration of the adsorbed enzyme with solutions containing 1000 μM nitrite the reversible reduction of the high-spin heme was described by *E_m* = -300 ± 15 mV. This value is approximately 300 mV lower than that resolved in the absence of added nitrite, namely, -15 ± 15 mV. Thus, the behavior is fully consistent with the higher affinity of nitrite for oxidized as compared to reduced forms of the enzyme. When the experiment was repeated with solutions containing 5 or 50 μM nitrite the oxidation state of the high-spin heme failed to equilibrate with the applied potential on the time-scale of the experiment. By contrast redox transformation of the low-spin hemes proceeded reversibly and could be described by *E_m* values of +15, -135, -200 and -320 mV (all values ±15 mV) that are in reasonable agreement with the values of +22, -117, -189, and -275 mV reported for *Ec* NrfA²⁸.

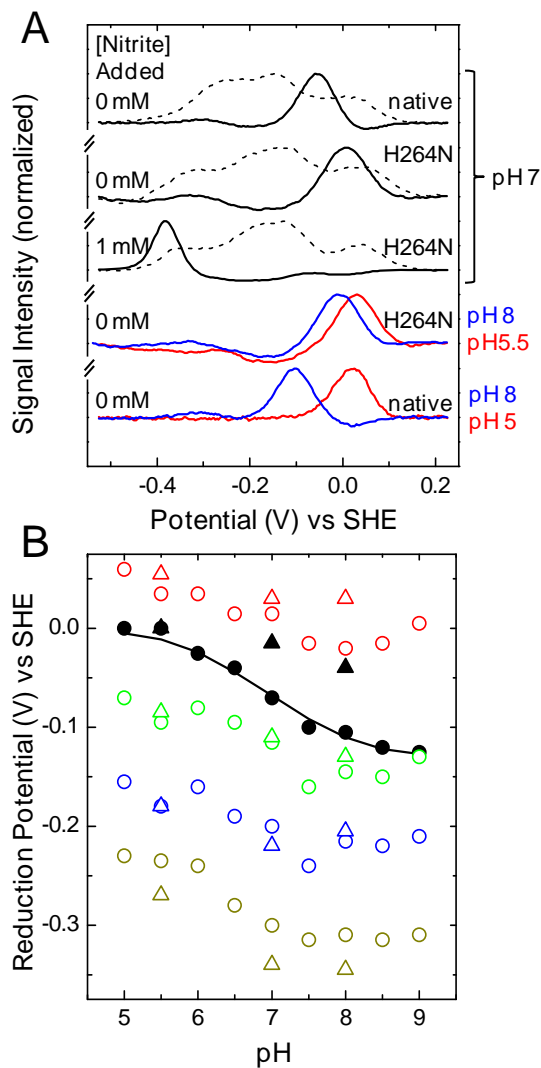


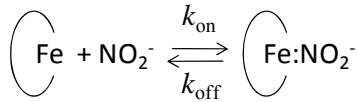
Figure 5. Spectroelectrochemical characterization of His264Asn and native *E. coli* NrfA enzymes adsorbed on mesoporous SnO₂ electrodes. (A) Redox activity of the high-spin (continuous lines) and low-spin hemes (broken lines) visualized by the absorbance change at 442 and 552 nm respectively during a scan to increasingly negative potential at 5 mV s⁻¹ for the indicated enzyme, nitrite concentration and pH. Data presented as first derivative of the absorbance with applied potential (*dA/dE*). (B) pH dependence of the reduction potentials of the high-spin (filled symbols) and low-spin (open symbols) hemes for His264Asn (triangles) and native (circles) NrfA. The line shows the behavior predicted for an *n* = 1 center with *E_{alk}* = -130 mV that binds a single proton with *pK_a^{red}* = 8.1, *pK_a^{ox}* = 5.8, see text for details.

Greater insight into the behavior of the high-spin heme in solutions of 5 or 50 μM nitrite was obtained when the protein film was poised for 3 minutes at a defined potential and the absorbance spectrum measured to quantify the population of ferrous heme. Plotting this population as a function of electrode potential when the film was exposed to a series of increasingly negative potentials and then a series of increasingly positive potentials revealed clear hysteresis in the reductive and oxidative behaviors, Fig. 6A. This is most readily explained by a square-scheme describing coupled

binding of nitrite and an electron to the active site, Fig. 7A. Reduction of the high-spin heme is centered on -300 mV in solutions of 5, 50 and 1000 μM nitrite indicating that the release of nitrite is slow until the ferrous active site is formed. Reoxidation of the heme occurs at more positive potentials for the lower nitrite concentrations. This reveals that nitrite binding is slow until the ferric active site is formed. Thus, during cyclic voltammetry the binding of nitrite and electrons proceeds in a clockwise direction around the scheme illustrated in Fig. 7A and in full agreement with the predictions made on the basis of the hysteretic catalytic current-potential profiles describing hydroxylamine reduction by *Ec* His264Asn NrfA adsorbed on graphite electrodes, Fig. 2A and Supporting Information Fig. 2.

Results from the various methods used to study *Ec* His264Asn NrfA are in excellent qualitative agreement with regard to the description of nitrite (un-)binding the active site. We note that higher affinities for nitrite binding to *Ec* His264Asn NrfA are suggested when the enzyme is adsorbed on SnO_2 electrodes than when the enzyme is adsorbed on graphite electrodes or in solution and this can be attributed to nitrite partitioning into the mesoporous SnO_2 material³⁶. This, together with restricted rates of diffusion within the mesoporous SnO_2 structure³⁷, precludes the use of SnO_2 electrodes in experiments to quantify rates of nitrite (un-)binding. Instead these rates were defined through changes in the catalytic currents displayed by *Ec* His264Asn NrfA adsorbed on rapidly rotating graphite electrodes. Chronoamperometry was employed for this purpose because it has the advantage of avoiding the intimate linkage of time and electrochemical potential that is intrinsic to cyclic voltammetry, Fig. 6B.

The catalytic current arising from a film of *Ec* His264Asn NrfA poised at -550 mV in 10 mM hydroxylamine and various nitrite concentrations was seen to diminish slowly after stepping to -275 mV. Thus, nitrite binding to the enzyme, as visualized by inhibition of hydroxylamine reduction, occurs slowly after being triggered by the step to higher potential. In the simplest case reversible binding of nitrite to the enzyme is described as



where binding and dissociation are first order in each reactant. The concentration of nitrite greatly exceeds the population of electroactive enzyme in these experiments. As a consequence the time-dependence of the catalytic current at -275 mV can be related to the population of nitrite bound enzyme through the relationship:

$$\begin{aligned} \ln(i_{\text{cat}}^{\text{eq}} - i_{\text{cat}}^t) &= \ln([\text{Fe}:\text{NO}_2^-]^{\text{eq}} - [\text{Fe}:\text{NO}_2^-]^t) \\ &= \ln[\text{Fe}:\text{NO}_2^-]^{\text{eq}} - k_{\text{eff}} t \end{aligned}$$

where $k_{\text{eff}} = k_{\text{on}}[\text{NO}_2^-] + k_{\text{off}}$ and the superscripts eq and t refer to equilibrated and at time t, respectively. For each nitrite concentration the current observed after stepping to -275 mV is well described by this relationship, e.g., Fig. 6B inset left. The plot of k_{eff} versus nitrite concentration is linear yielding

$k_{\text{on}} = 0.12 \pm 0.05 \text{ mM}^{-1} \text{ s}^{-1}$ and $k_{\text{off}} = 0.04 \pm 0.01 \text{ s}^{-1}$, Fig. 6B, inset right.

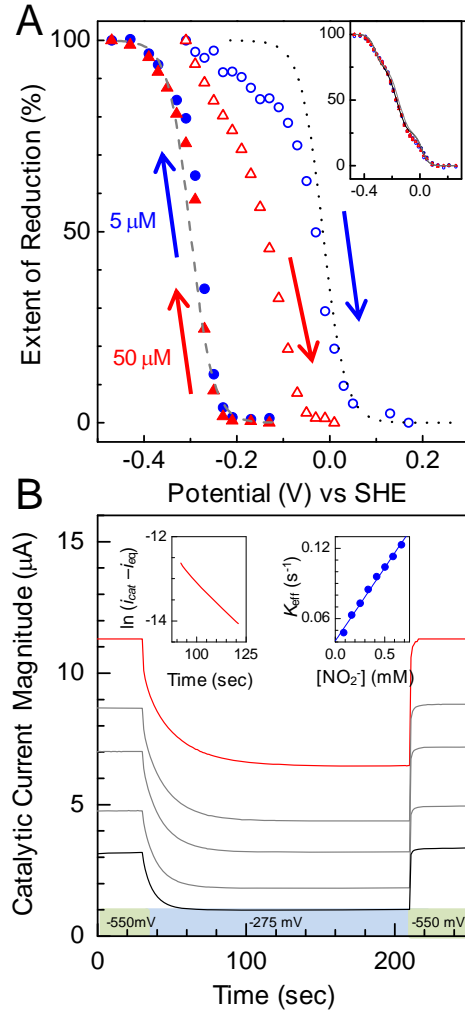


Figure 6. Redox-linked nitrite (un-)binding of *Ec* His264Asn NrfA. (A) Hysteresis in the redox titration of the high-spin heme in *Ec* His264Asn NrfA adsorbed on SnO_2 electrodes induced by the presence of 5 μM nitrite (blue points) and 50 μM nitrite (red points) at 4 $^\circ\text{C}$. The extent of high-spin heme reduction is shown for the reductive (closed symbols) and oxidative (open symbols) titres as defined by $A_{442\text{nm}} - A_{452\text{nm}}$ at each potential. The Nernstian behavior measured in the absence of added nitrite (dotted black line) and the presence of 1 mM nitrite (dashed grey line) are shown for reference. Inset: equivalent data for the low-spin hemes as defined by $A_{552\text{nm}} - A_{582\text{nm}}$ at each potential and showing essentially identical, Nernstian titration of these centers in all four conditions. (B) Catalytic current magnitudes resolved for a film of *Ec* His264Asn NrfA in 10 mM hydroxylamine on a graphite electrode rotating at 3k rpm during chronoamperometry at 20 $^\circ\text{C}$ with an applied electrode potential of -550 and -275 mV as indicated. The concentration of nitrite added (mM) was 0.084 (red) and 0.167, 0.251, 0.418 and 0.669 (black lines). Insets: representative plot for the determination of k_{eff} (left, 0.084 mM nitrite) and the kinetic parameters k_{on} and k_{off} describing nitrite (un-)binding (right), see text for details. Buffer-electrolyte 2 mM CaCl_2 , 50 mM HEPES, pH 7.

At -275 mV the prevailing oxidation state of the nitrite bound active site is Fe(III) while that of the nitrite unbound form is Fe(II) when not engaged in catalytic transformation of hydroxylamine. As a consequence these rate constants describe the corresponding diagonal transition across the square-scheme of Fig. 7A. The frequency of hydroxylamine reduction ($>3000\text{ s}^{-1}$) places a plausible lower limit on rates of electron transfer through the enzyme. Thus it appears that binding and release of nitrite, rather than electrons, is rate limiting in these processes and occurs more slowly than in the native enzyme. Full simulation of the cyclic voltammetric response to yield rate constants for each side of the square-scheme was precluded by two factors. These were the outcomes of a detailed consideration of the experimentally defined E_m and K_d values, described below, and the intrinsic complexity of the catalytic-current potential profile observed at low(negligible) nitrite concentrations.

DISCUSSION

Hemoproteins reduce nitrite to either nitric oxide or ammonium and long-standing interest in the mechanisms of these reactions has been reinvigorated by our growing understanding of the importance of this chemistry to the physiology of higher organisms¹. Wide-ranging systems have aimed to capture the key features of such catalysis but their development is often impeded by a lack of information regarding the catalytic contributions made by individual amino acids. We have provided here unprecedented insight into the catalytic roles played by the distal His of cytochrome *c* nitrite reductases. In closing three aspects of our findings deserve further comment, namely, the failure of *Ec* His264Asn NrfA to reduce bound nitrite, the contributions of the distal His to nitrite reduction in native enzyme and the wider implications of the thermodynamic parameters describing electron and nitrite binding to *Ec* His264Asn NrfA. Given the frequency with which His features in the active sites of metallo-enzymes and the central role of coupled electron/ligand binding events in redox catalysis these observations are of relevance to catalytic and regulatory mechanisms operating in many enzymes.

A striking finding of this study is that *Ec* His264Asn NrfA, despite simultaneously binding electrons and nitrite, fails to catalyze nitrite reduction at a detectable rate. Because hydroxylamine reduction by *Ec* His264Asn NrfA occurs with a similar turnover frequency to the native enzyme there is no indication that the rates of electron- or proton-transfer to the active-site in the variant enzyme are significantly compromised. As a consequence it can be proposed that the distal His has two key roles in nitrite reduction, namely, to ensure rapid binding of nitrite and then to orient the bound nitrite for reductive N-O bond cleavage. With regard to the rate of nitrite binding, the distal His is positioned with its side chain facing the catalytic heme and the crystallographic data sets provide no indication for conformational flexibility. As a consequence this His is more likely to facilitate the chemical association of nitrite and heme than nitrite diffusion along the solvent-filled channels linking the active site and bulk solvent.

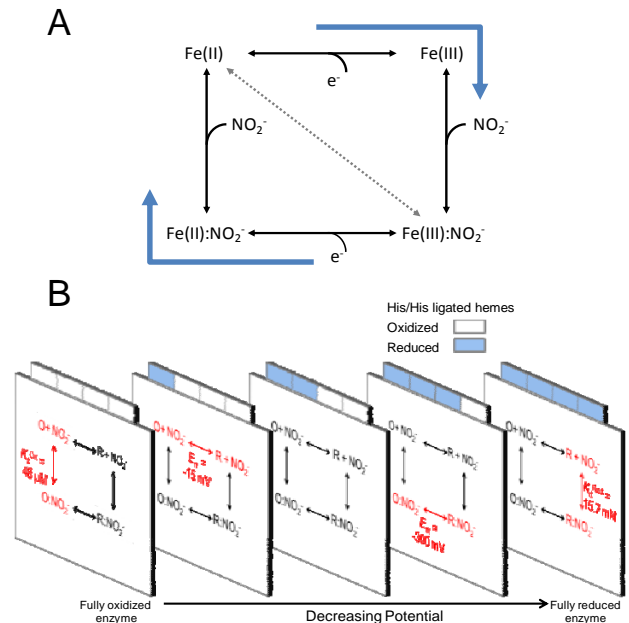


Figure 7. Thermodynamic descriptions of electron- and nitrite-binding to the active site of *Ec* His264Asn NrfA. (A) Square-scheme presenting the simplest description of electron- and nitrite-binding at the active-site heme. The blue arrows illustrate progress round the scheme during cyclic voltammetry. The broken arrow describes the prevailing process on stepping from -550 to -275 mV during chronoamperometry. See text for further details. (B) Extension of the square-scheme presented in (A) to account for modulation of the thermodynamic properties by redox transformation of the neighboring His/His ligated hemes. Ferric and ferrous states of the catalytic heme represented by O and R respectively. Processes corresponding to the experimentally determined E_m and K_d values are illustrated (red) for the square-scheme that best describes the prevailing oxidation states of the low-spin hemes, see text for details.

In an attempt to resolve the orientation of nitrite bound to *Ec* His264Asn NrfA we soaked crystals of this enzyme in cryoprotectant containing 50 mM nitrite prior to cooling in liquid N_2 . The crystals diffracted to 2.2 Å resolution and displayed additional electron density on the distal face of the catalytic heme when compared to those prepared in the absence of added nitrite. Modeling this density as water produces residual positive density. This is indicative of the presence of a larger molecule that is most likely to be nitrite as predicted by the optical spectroscopy. However, the relevant electron densities in the two subunits of the unit cell were different and it proved impossible to resolve conclusively the orientation of the bound nitrite in either. In one subunit the electron density was better described by an Fe-ONO nitrito-species. In the other subunit the density could also accommodate the Fe-NO₂ nitro-species. Thus, the bound nitrite may exist as linkage isomers similar to those resolved in Fe-porphyrin model compounds³⁸⁻⁴¹. Clearly a distal pocket comprised of Asn, Arg and Tyr as found in *Ec* His264Asn NrfA fails to provide sufficient H-bonding opportunities and/or steric constraints to impose a unique orientation on bound nitrite. In myoglobin the specific H-bonding opportunities provided by the distal pocket determine whether

nitrite is bound in the nitrito- or nitro-mode⁴². The same appears to be true for cytochrome *c* nitrite reductases.

Whether the H-bonding opportunities afforded by the distal His in native cytochrome *c* nitrite reductases are in themselves sufficient to impose a single orientation on the bound nitrite remains to be established. However, it seems likely that such H-bonding will be favored when the distal His is protonated. Indeed we predict that this will be the case for the acidic conditions where nitro-bound nitrite, H-bonded to the distal His, was resolved in cytochrome *c* nitrite reductases from *W. succinogenes* and *Thioalkalivibrio nitratireducens*^{13,15}. Reduction of the catalytic heme, triggering protonation of the distal His to correctly orient bound nitrite for N-O bond cleavage may facilitate nitrite ammonification. At least one His/His-ligated heme has a reduction potential above that of the catalytic center. Orienting nitrite for N-O bond cleavage when two electrons are present in the enzyme would minimize the accumulation of an intermediate one-electron more reduced than the substrate.

Finally we turn to consider the thermodynamic parameters describing nitrite- and electron-binding to *Ec* His264Asn NrfA. Two dissociation constants and two reduction potentials describe these events within the square-scheme of Fig. 7A. With knowledge of three of these parameters the fourth should be predictable from a consideration of the free energy change associated with each side of the square. Applying this approach to the experimentally determined K_d^{ox} and E_m values predicts K_d^{red} to be of the order of 7000 mM and so well outside the error associated with the experimentally determined value of 15 mM. This is most likely to be a consequence of the need to study *Ec* His264Asn NrfA across a potential window of some 0.4 V in order to address the ferric and ferrous states of the catalytic heme. The low-spin hemes undergo redox transformations across this potential window and we propose that their oxidation states impact on electron and nitrite binding to the catalytic heme. In the extreme situation redox transformation of each His/His ligated heme would impact on the K_d and E_m values of the catalytic heme such that a series of five square-schemes would be needed to describe these parameters. This is illustrated in Fig. 7B where the transitions most likely to be represented by the experimentally determined parameters are seen to lie in different planes.

Much attention is focused on defining the determinants of catalytic rate in multi-centered redox enzymes. It is well-established that the proximity of adjacent redox centers and the potential differences between them make significant contributions to the rates of intraprotein electron transfer^{43,44}. The work presented here adds to this discussion by demonstrating that substrate binding events may also be modulated by the prevailing oxidation state(s) of neighboring center(s). Such behavior may contribute to the complex catalytic current-potential relationships displayed by multi-centered redox enzymes, including cytochrome *c* nitrite reductase, where multi-phasic modulations of catalytic rate are induced by change of electrode potential, see for example^{45,46} and references therein.

In conclusion, a combination of electrochemistry, spectroscopy, X-ray diffraction and protein engineering have provided unprecedented resolution of catalytic contributions made by the distal His in cytochrome *c* nitrite reductases. This

residue is seen to play a crucial role in the early steps of nitrite reduction but to make very little contribution to the proposed final step in this process, namely, hydroxylamine reduction. In addition the His to Asn variant has provided evidence that the prevailing oxidation states of the His/His ligated hemes impact on electron- and ligand-binding within the active site in behavior that has implications for interpreting the catalytic properties of multi-centered redox enzymes.

ASSOCIATED CONTENT

The preparation of *Ws* His277Asn NrfA together with details of the structure determination and voltammetric characterization and spectropotentiometric titration of *Ec* His264Asn NrfA are supplied as Supporting Information. This material is available free of charge via the Internet at <http://pubs.acs.org>.

AUTHOR INFORMATION

Corresponding Author

* j.butt@uea.ac.uk; School of Chemistry, University of East Anglia, Norwich Research Park, NR4 7TJ, UK

Present Addresses

† Aix Marseille University, CNRS, BIP UMR 7281, F-13402 Marseille 20, France

Author Contributions

The manuscript was written through contributions of all authors. All authors have given approval to the final version of the manuscript.

Funding Sources

The work was funded by the UK Biotechnology and Biosciences Research Council (B18695 and BB/C007808 to DJR, MRC and JNB), the Deutsche Forschungsgemeinschaft (grant S1 848/5-1 to JS), and the University of East Anglia through a PhD studentship to CWJL.

ACKNOWLEDGMENT

We are grateful to Professor Jeff Cole (Birmingham, UK) for provision of the *E. coli* strain producing *Ec* His264Asn NrfA, Verity Lyall for assistance with protein purification, Gemma Kemp and Sam Dalziel (University of East Anglia) for assistance defining the redox properties of *Ec* NrfA and rates of nitrite (un-)binding, Dr Marcus Edwards (University of East Anglia, UK) for assistance with protein structure determination and Professor James Durrant and Dr Li Xiaoe (Imperial College London) for providing SnO₂ electrodes.

ABBREVIATIONS

Ec, *Escherichia coli*; E_m , midpoint potential; EPR, electron paramagnetic resonance; k_{cat} , turnover frequency; K_M , Michaelis constant; LMCT, ligand-to-metal charge-transfer; NrfA, penta-heme cytochrome *c* nitrite reductase; *Ws*, *Wolinella succinogenes*.

REFERENCES

- (1) Maia, L. B.; Moura, J. J. G. *Chem. Rev.* **2014**, *114*, 5273-5357.
- (2) Zumft, W. G. *Microbiol. Mol. Biol. Rev.* **1997**, *61*, 533-616.
- (3) Rees, D. C.; Tezcan, F. A.; Haynes, C. A.; Walton, M. Y.; Andrade, S.; Einsle, O.; Howard, J. B. *Phil. Trans. Roy. Soc. A* **2005**, *363*, 971-984.

- (4) Schumacher, W.; Hole, U.; Kroneck, M. H. *Biochem. Biophys. Res. Commun.* **1994**, *205*, 911-916.
- (5) Pereira, I. C.; Abreu, I. A.; Xavier, A. V.; LeGall, J.; Teixeira, M. *Biochem. Biophys. Res. Commun.* **1996**, *224*, 611-618.
- (6) Tikhonova, T. V.; Slutsky, A.; Antipov, A. N.; Boyko, K. M.; Polyakov, K. M.; Sorokin, D. Y.; Zvyagil'skaya, R. A.; Popov, V. O. *Biochim. Biophys. Acta* **2006**, *1764*, 715-723.
- (7) Youngblut, M.; Judd, E. T.; Srajer, V.; Sayyed, B.; Goelzer, T.; Elliott, S. J.; Schmidt, M.; Pacheco, A. A. *J. Biol. Inorg. Chem.* **2012**, *17*, 647-662.
- (8) Bamford, V. A.; Angove, H. C.; Seward, H. E.; Thomson, A. J.; Cole, J. A.; Butt, J. N.; Hemmings, A. M.; Richardson, D. J. *Biochemistry* **2002**, *41*, 2921-2931.
- (9) Einsle, O.; Stach, P.; Messerschmidt, A.; Simon, J.; Kröger, A.; Huber, R.; Kroneck, P. M. H. *J. Biol. Chem.* **2000**, *275*, 39608-39616.
- (10) Einsle, O.; Messerschmidt, A.; Stach, P.; Bourenkov, G. P.; Bartunik, H. D.; Huber, R.; Kroneck, P. M. H. *Nature* **1999**, *400*, 476-480.
- (11) Rodrigues, M. L.; Oliveira, T. F.; Pereira, I. A. C.; Archer, M. *EMBO J.* **2006**, *25*, 5951-5960.
- (12) Cunha, C. A.; Macieira, S.; Dias, J. M.; Almeida, G.; Goncalves, L. L.; Costa, C.; Lampreia, J.; Huber, R.; Moura, J. J. G.; Moura, I.; Romao, M. J. *J. Biol. Chem.* **2003**, *278*, 17455-17465.
- (13) Polyakov, K. M.; Boyko, K. M.; Tikhonova, T. V.; Slutsky, A.; Antipov, A. N.; Zvyagil'skaya, R. A.; Popov, A. N.; Bourenkov, G. P.; Lamzin, V. S.; Popov, V. O. *J. Molec. Biol.* **2009**, *389*, 846-862.
- (14) Welsh, A.; Chee-Sanford, J. C.; Connor, L. M.; Löffler, F. E.; Sanford, R. A. *App. Environ. Microbiol.* **2014**, *80*, 2110-2119.
- (15) Einsle, O.; Messerschmidt, A.; Huber, R.; Kroneck, P. M. H.; Neese, F. *J. Am. Chem. Soc.* **2002**, *124*, 11737-11745.
- (16) Bykov, D.; Neese, F. *J. Biol. Inorg. Chem.* **2011**, *16*, 417-430.
- (17) Bykov, D.; Neese, F. *J. Biol. Inorg. Chem.* **2012**, *17*, 741-760.
- (18) Bykov, D.; Plog, M.; Neese, F. *J. Biol. Inorg. Chem.* **2014**, *19*, 97-112.
- (19) Clarke, T. A.; Kemp, G. L.; Van Wonderen, J. H.; Doyle, R. M. A. S.; Cole, J. A.; Tovell, N.; Cheesman, M. R.; Butt, J. N.; Richardson, D. J.; Hemmings, A. M. *Biochemistry* **2008**, *47*, 3789-3799.
- (20) Arslan, E.; Schulz, H.; Zufferey, R.; Kunzler, P.; Thöny-Meyer, L. *Biochem. Biophys. Res. Commun.* **1998**, *251*, 744-747.
- (21) Clarke, T. A.; Mills, P. C.; Pooock, S. R.; Butt, J. N.; Cheesman, M. R.; Cole, J. A.; Hinton, J. C. D.; Hemmings, A. M.; Kemp, G.; Soderberg, C. A. G.; Spiro, S.; Van Wonderen, J.; Richardson, D. J. *Meth. Enzymol.* **2008**, *437*, 63-77.
- (22) Kern, M.; Simon, J. *Meth. Enzymol.* **2011**, *486*, 429-446.
- (23) Winter, G. *J. App. Cryst* **2009**, *43*, 186-190.
- (24) Collaborative Computational Project, N. *Acta Cryst. D* **1994**, *43*, 760-763.
- (25) Angove, H. C.; Cole, J. A.; Richardson, D. J.; Butt, J. N. *J. Biol. Chem.* **2002**, *277*, 23374-23381.
- (26) Kemp, G. L.; Clarke, T. A.; Marritt, S. J.; Lockwood, C.; Pooock, S. R.; Hemmings, A. M.; Richardson, D. J.; Cheesman, M. R.; Butt, J. N. *Biochem. J.* **2010**, *431*, 73-80.
- (27) Gwyer, J. D.; Richardson, D. J.; Butt, J. N. *J. Am. Chem. Soc.* **2005**, *127*, 14964-14965.
- (28) Marritt, S. J.; Kemp, G. L.; Xiaoe, L.; Durrant, J. R.; Cheesman, M. R.; Butt, J. N. *J. Am. Chem. Soc.* **2008**, *130*, 8588-8589.
- (29) Liu, M. C.; Liu, M. Y.; Payne, W. J.; Peck, H. D.; LeGall, J. *FEMS Microbiol. Letts* **1983**, *19*, 201-206.
- (30) Judd, E. T.; Stein, N.; Pacheco, A. A.; Elliott, S. J. *Biochemistry* **2014**, *53*, 5638-5646.
- (31) Gwyer, J. D.; Angove, H. C.; Richardson, D. J.; Butt, J. N. *Bioelectrochem.* **2004**, *63*, 43-47.
- (32) Cheesman, M. R.; Watmough, N. J.; Gennis, R. B.; Greenwood, C.; Thomson, A. *J. Eur. J. Biochem.* **1994**, *219*, 595-602.
- (33) Burlat, B.; Gwyer, J. D.; Pooock, S.; Clarke, T.; Cole, J. A.; Hemmings, A. M.; Cheesman, M. R.; Butt, J. N.; Richardson, D. J. *Biochem. Soc. Trans.* **2005**, *33*, 137-140.
- (34) van Wonderen, J. H.; Burlat, B.; Richardson, D. J.; Cheesman, M. R.; Butt, J. N. *J. Biol. Chem.* **2008**, *283*, 9587-9594.
- (35) Almeida, M. G.; Silveira, C. M.; Guigliarelli, B.; Bertrand, P.; Moura, J. J. G.; Moura, I.; Léger, C. *FEBS Letts* **2007**, *581*, 284-288.
- (36) Renault, C.; Andrieux, C. P.; Tucker, R. T.; Brett, M. J.; Balland, V.; Limoges, B. *J. Am. Chem. Soc.* **2012**, *134*, 6834-6845.
- (37) McMillan, D. G. G.; Marritt, S. J.; Kemp, G. L.; Gordon-Brown, P.; Butt, J. N.; Jeuken, L. J. C. *Electrochim Acta* **2013**, *110*, 79-85.
- (38) Nasri, H.; Ellison, M. K.; Chen, S. X.; Huynh, B. H.; Scheidt, W. R. *J. Am. Chem. Soc.* **1997**, *119*, 6274-6283.
- (39) Lee, J.; Kovalevsky, A. Y.; Novozhilova, I. V.; Bagley, K. A.; Coppens, P.; Richter-Addo, G. B. *J. Am. Chem. Soc.* **2004**, *126*, 7180-7181.
- (40) Novozhilova, I. V.; Coppens, P.; Lee, J.; Richter-Addo, G. B.; Bagley, K. A. *J. Am. Chem. Soc.* **2006**, *128*, 2093-2104.
- (41) Silaghi-Dumitrescu, R. *Inorg. Chem.* **2004**, *43*, 3715-3718.
- (42) Yi, J.; Safo, M. K.; Richter-Addo, G. B. *Biochemistry* **2008**, *47*, 8247-8249.
- (43) Page, C. C.; Moser, C. C.; Chen, X. X.; Dutton, P. L. *Nature* **1999**, *402*, 47-52.
- (44) Kurnikov, I. V.; Ratner, M. A.; Pacheco, A. A. *Biochemistry* **2005**, *44*, 1856-1863.
- (45) Hexter, S. V.; Esterle, T. F.; Armstrong, F. A. *PhysChemChem-Phys* **2014**, *16*, 11822-11833.
- (46) Léger, C.; Bertrand, P. *Chem. Rev.* **2008**, *108*, 2379-2438.

FOR TABLE OF CONTENTS ONLY

